Released-phase quantum Monte Carlo method

Matthew D. Jones,[1,2,*] Gerardo Ortiz,[2,*] and David M. Ceperley[1,2]
[1]*National Center for Supercomputing Applications, University of Illinois at Urbana-Champaign, 1110 West Green Street, Urbana, Illinois 61801*
[2]*Department of Physics, University of Illinois at Urbana-Champaign, 1110 West Green Street, Urbana, Illinois 61801*
(Received 18 November 1996)

The correlation function Monte Carlo method for calculating ground and excited state properties is extended to complex Hamiltonians and used to calculate the spectrum of neutral helium in a wide range of magnetic fields, a system of particular interest in astrophysics. Correlation functions in imaginary time are evaluated for a set of trial functions over a random walk whose dynamics is governed by the imaginary-time Schrödinger equation. Estimates of the exact energy spectrum and other expectations are made by diagonalizing the matrix of correlation functions. Using the exact results of this ''released-phase'' Monte Carlo approach, we assess the accuracy of the fixed-phase quantum Monte Carlo and Hartree-Fock methods for the helium atom in strong magnetic fields. [S1063-651X(97)07605-8]

PACS number(s): 02.70.Lq, 31.10.+z, 32.60.+i, 71.10.−w

I. INTRODUCTION

If the Hamiltonian of a physical system is real, then it is always possible to construct wave functions that are real. With the addition of a magnetic field the ground state will, in general, be complex valued. Quantum Monte Carlo simulation is difficult unless the wave function can be made real and non-negative because the wave function is interpreted as a probability distribution. For real-valued wave functions one uses the *fixed-node* [1] approximation to calculate states which are the ground states of a given symmetry but are not positive. For complex-valued states, the analogous method is the *fixed-phase* quantum Monte Carlo (FP) technique developed by Ortiz and co-workers [2,3]. It assumes a *trial phase* of the complex many-body wave function, and exactly solves the resulting equation for its modulus using random walks.

As is the case with the fixed-node approximation, one does not know internally the quality of the trial phase. For real wave functions one can calculate the exact energy by allowing the walks to cross the nodal surface. There are two related methods for relaxing the fixed-node constraint in this fashion, called the transient estimate and the release-node methods. For estimating excited states, one must also keep the states orthogonal to lower states of the same symmetry. This is accomplished by a method called correlation function Monte Carlo, introduced by Ceperley and Bernu [4] (hereafter referred to as CB), and applied to small molecules [5] and the excitations of the two dimensional electron gas [6]. It has also been used to determine eigenvalues of classical spin systems [7]. An advantage of this method is that one can simultaneously calculate properties of many excited states with a single random walk.

In this article we discuss how to extend the correlation function method to include complex Hamiltonians and wave functions, and apply this new approach to the case of an isolated helium atom in a very strong magnetic field. One can view this extension of the correlation function approach as a relaxation of the fixed-phase constraint (hence, ''released-phase''), while simultaneously evaluating many excited states. We first review the CB technique and discuss the changes that need to be made in the method to treat complex-valued Hamiltonians and wave functions. Sample calculations using the released-phase (RP) Monte Carlo method are then presented for helium atoms in a magnetic field, which to date have only been studied with relatively inaccurate mean-field methods.

Neutral helium has been suggested as a possible explanation for unexplained spectra of some magnetic white dwarf stars [8,9], where the field can be as strong as 10^{11} G. Previous calculations for helium in strong magnetic fields using Hartree-Fock (HF) [10,12] methods have not been sufficiently accurate, and the fixed-phase method is no longer variational for excited states. Two electron systems also occur as excitons in certain semiconductors [13]. We use our application to magnetized helium atoms to study the efficiency of the released-phase quantum Monte Carlo approach.

Although in this paper we focus on helium, the RP method is sufficiently general for application to any problem with a spectrum of complex valued eigenstates, such as quantum dots [14] and anyons in a magnetic field [15,16].

II. THE CORRELATION FUNCTION MONTE CARLO METHOD

Zero temperature quantum Monte Carlo (MC) methods typically begin with the choice of the trial wave function. Here we are interested in ground *and* excited states, so we begin by choosing a basis of trial wave functions that represent our best (analytic) approximation to the spectrum of states that we wish to examine. In the correlation function MC method, one projects this basis with the exponential of the Hamiltonian operator using random walks. Matrices formed by the resulting autocorrelation functions evaluated during the random walk are then solved for the energy spectrum and other properties. The eigenvalues converge to the exact energies of the system in the limit of infinite imaginary

*Present address: Theoretical Division, T-11 MS B262, Los Alamos National Laboratory, Los Alamos, NM 87545.

time, but the variance of the energy grows both exponentially in time and excitation energy. Thus, in practice, this method is limited by the size of the system and the number of excitations of a given symmetry. Our presentation of the correlation function method is necessarily brief; see Ref. [4] for further details of the method. Here we introduce the formalism required for complex Hamiltonians.

Given a basis set $\{f_j\}$ of m linearly independent states which approximate the lowest energy states of our system, the exact eigenfunctions can be approximated in terms of this basis,

$$\Phi_i(\mathbf{R},0)=\sum_{j=1}^{m} d_{ij} f_j(\mathbf{R}), \tag{1}$$

where $\mathbf{R}=(\mathbf{r}_1,\mathbf{r}_2,\ldots,\mathbf{r}_N)$ represents a point in the configuration space of N particles. The variational theorem asserts that upper bounds [17] to the exact energies E_i^{ex}, can be determined by finding the stationary points of the Rayleigh quotient

$$\Lambda_i(0)=\frac{\int d\mathbf{R}\Phi_i^*(\mathbf{R},0)\hat{H}\Phi_i(\mathbf{R},0)}{\int d\mathbf{R}\Phi_i^*(\mathbf{R},0)\Phi_i(\mathbf{R},0)}, \tag{2}$$

with respect to the coefficients d_{ij} ($\hat{H}$ is the Hamiltonian of the system under consideration). The size of the basis set m determines the maximum number of excited state energies that can be bounded.

Let us use the imaginary time density matrix to find a new basis,

$$\{\tilde{f}_i\}(\mathbf{R},t)=\{e^{-t\hat{H}/2}f_i\}(\mathbf{R},t), \tag{3}$$

a basis in which the higher energy components have been reduced relative to the lowest energy states as t increases. If we make $\Lambda_i(t)$ stationary with respect to the expansion coefficients $\{d_{ij}(t)\}$, we arrive at a matrix equation for each eigenvector $\mathbf{d}_i^{\mathrm{T}}=(d_{i1},d_{i2},\ldots,d_{im})$,

$$\mathbf{H}\mathbf{d}_i=\Lambda_i\mathbf{S}\mathbf{d}_i, \tag{4}$$

where the matrices $\mathbf{H}$ and $\mathbf{S}$ are given by

$$\mathbf{H}_{jk}(t)=\int d\mathbf{R}d\mathbf{R}' f_j^*(\mathbf{R})\langle\mathbf{R}|\hat{H}e^{-t\hat{H}}|\mathbf{R}'\rangle f_k(\mathbf{R}'), \tag{5}$$

$$\mathbf{S}_{jk}(t)=\int d\mathbf{R}d\mathbf{R}' f_j^*(\mathbf{R})\langle\mathbf{R}|e^{-t\hat{H}}|\mathbf{R}'\rangle f_k(\mathbf{R}'). \tag{6}$$

Solving Eq. (4) allows us to project out the lowest m energy states while simultaneously enforcing orthogonality through the generalized eigenproblem process.

To reduce the statistical variance in the Monte Carlo evaluation of $\mathbf{H}$ and $\mathbf{S}$ one introduces importance sampling by multiplying and dividing by a guiding function ψ_G. We will assume that ψ_G is normalized. The importance-sampled Green's function is given by

$$G(\mathbf{R},\mathbf{R}';t)=\psi_G(\mathbf{R})\langle\mathbf{R}|e^{-t\hat{H}}|\mathbf{R}'\rangle\psi_G^{-1}(\mathbf{R}'), \tag{7}$$

where ψ_G is a real valued, non-negative function. The matrices in terms of G then become

$$\mathbf{H}_{jk}(t)=\int d\mathbf{R}d\mathbf{R}' F_j^*(\mathbf{R})G(\mathbf{R},\mathbf{R}';t) \times E_k(\mathbf{R}')F_k(\mathbf{R}')\psi_G^2(\mathbf{R}'), \tag{8}$$

$$\mathbf{S}_{jk}(t)=\int d\mathbf{R}d\mathbf{R}' F_j^*(\mathbf{R})G(\mathbf{R},\mathbf{R}';t)F_k(\mathbf{R}')\psi_G^2(\mathbf{R}'), \tag{9}$$

where $F_i=f_i/\psi_G$ and $E_i=f_i^{-1}\hat{H}f_i$ is the local energy of the individual basis states. Note that E_i is in general a complex-valued function of $\mathbf{R}$.

Because the Green's function is an exponential operator, we can expand it in terms of an Euclidean path integral

$$G(\mathbf{R},\mathbf{R}';t)=\int d\mathbf{R}_1\ldots d\mathbf{R}_{n-1}\prod_{j=1}^{n} G(\mathbf{R}_j,\mathbf{R}_{j-1};\tau), \tag{10}$$

where $\mathbf{R}_0=\mathbf{R}'$, $\mathbf{R}_n=\mathbf{R}$ (the complete path consists of n individual steps), and $t=n\tau$. At sufficiently large n (small τ) we can write down accurate approximations to the Green's function, and sample it with diffusion Monte Carlo.

During the random walk we sample from a diffusion Green's function $G_d(R_j,R_{j-1};\tau)$ with a time interval τ, iteratively constructing a trajectory of configurations $\{\mathbf{R}_1,\ldots,\mathbf{R}_p\}$. ($p$ is the total length of the random walk), distributed according to the distribution

$$\mathcal{P}(\mathbf{R}_l)=\psi_G^2(\mathbf{R}_0)\prod_{j=1}^{l} G_d(\mathbf{R}_j,\mathbf{R}_{j-1};\tau), \tag{11}$$

where $l\leqslant n$. The matrices are evaluated over the course of each trajectory as

$$\mathbf{H}_{jk}(l\tau)=\int d\mathbf{R}_0\ldots d\mathbf{R}_l\mathbf{h}_{jk}(l\tau)\mathcal{P}(\mathbf{R}_l), \tag{12}$$

$$\mathbf{S}_{jk}(l\tau)=\int d\mathbf{R}_0\ldots d\mathbf{R}_l\mathbf{s}_{jk}(l\tau)\mathcal{P}(\mathbf{R}_l). \tag{13}$$

A single random walk can compute all of the matrix elements simultaneously, the correlation between the fluctuations in $\mathbf{H}$ and $\mathbf{S}$ will reduce the statistical error of the estimated eigenvalue. The estimates of the matrices are then given by comparing Eqs. (12) and (13) with Eqs. (8) and (9),

$$\mathbf{h}_{jk}(l\tau)=\frac{1}{2(p-l)}\sum_{n=1}^{p-l} W_{n,n+l}F_j^*(\mathbf{R}_n)F_k(\mathbf{R}_{n+l}) \times[E_k(\mathbf{R}_{n+l})+E_j^*(\mathbf{R}_n)], \tag{14}$$

$$\mathbf{s}_{jk}(l\tau)=\frac{1}{p-l}\sum_{n=1}^{p-l} W_{n,n+l}F_j^*(\mathbf{R}_n)F_k(\mathbf{R}_{n+l}), \tag{15}$$

where

$$W_{n,n+l}=\prod_{i=1}^{l} G(\mathbf{R}_{n+i},\mathbf{R}_{n+i-1};\tau)/G_d(\mathbf{R}_{n+i},\mathbf{R}_{n+i-1};\tau). \tag{16}$$

Note that the weights $W_{n,n+l}$ will, in general, be complex valued.

Since the noise is not Hermitian, statistical fluctuations can be further reduced by using the Hermitian property of the matrices, symmetrizing as in

$$\mathbf{h}_{jk}=\tfrac{1}{2}(\mathbf{h}_{jk}+\mathbf{h}_{kj}^{*}), \tag{17}$$

applied directly to the estimator in Eq. (14). This recombination is equivalent to time reversing the path. The same trick is also applied to $\mathbf{s}_{jk}$ and Eq. (15).

The eigenvalues $\{\Lambda_i(t)\}$ converge monotonically $(\Lambda_i(t)\geqslant E_i^{ex},\forall t)$ to the exact energies $\{E_i^{ex}\}$ in the limit of infinite imaginary time,

$$\lim_{t\to\infty}\Lambda_i(t)=E_i^{ex}, \tag{18}$$

$$\frac{d\Lambda_i(t)}{dt}\leqslant 0, \quad \forall t. \tag{19}$$

The correlation function Monte Carlo method has the important zero variance property of the energy; as the basis set approaches the exact eigenstates, the variance of the estimates of the eigenvalues approaches zero.

A. The Green's function for charges in a magnetic field

Thus far we have described the general correlation function Monte Carlo method for ground and excited states. Here we discuss the principal changes that must be introduced to the method to accommodate complex-valued states. Specializing now in the case of nonrelativistic charges in an external vector potential $\mathbf{A}$ ($\nabla\times\mathbf{A}=\mathbf{B}$, where $\mathbf{B}$ is the external magnetic field), the Hamiltonian is (in hartree atomic units),

$$\hat{H}=\sum_{j=1}^{N}\frac{(\boldsymbol{\sigma}_j\cdot\boldsymbol{\Pi}_j)^2}{2}+V, \tag{20}$$

where $\boldsymbol{\sigma}_j$ denote Pauli spin matrices, $\boldsymbol{\Pi}=\mathbf{p}+\mathbf{A}$ is the kinetic momentum, and V is the total potential (which includes one- and two-body interactions). Without the loss of generality, we will only consider particles living in three spatial dimensions.

The importance-sampled Green's function [Eq. (7)] satisfies (in a gauge covariant form)

$$\partial_t G(\mathbf{R},\mathbf{R}';t)=-\frac{1}{2}\nabla_{\mathbf{R}}\{-\nabla_{\mathbf{R}}G+2G[\nabla_{\mathbf{R}}\ln(\psi_G)-i\mathbf{A}]\}-(E_L^{*}(\mathbf{R})-E_T)G, \tag{21}$$

where $\nabla_{\mathbf{R}}=\sum_{i=1}^{N}\nabla_{\mathbf{r}_i}$, $E_L=\psi_G^{-1}\hat{H}\psi_G$, and E_T is a trial energy, chosen to be real valued.

All but the term involving the vector potential of this expression for the Green's function (and the fact that E_L is complex valued) are commonly used in diffusion Monte Carlo. Trotter's theorem asserts that under weak conditions on the (linear) operators we can consider the evolution as the product of the evolution of each of the operators separately. Hence a short-time solution to Eq. (21) is given by the product of the three Green's functions [corrections are $\mathcal{O}(\tau^2)$],

$$G(\mathbf{R}_j,\mathbf{R}_{j-1};\tau)=G_d G_b G_{\mathbf{A}}, \tag{22}$$

where

$$G_d(\mathbf{R}_j,\mathbf{R}_{j-1};\tau)=(2\pi\tau)^{-3N/2}e^{-(\mathbf{R}_j-\mathbf{R}_{j-1}-\tau\mathbf{F}_Q(\mathbf{R}_{j-1}))^2/2\tau}, \tag{23}$$

$$G_b(\mathbf{R}_j,\mathbf{R}_{j-1};\tau)=e^{-\tau[(\tilde{E}_L(\mathbf{R}_j)+\tilde{E}_L(\mathbf{R}_{j-1}))/2-E_T]}, \tag{24}$$

$$G_{\mathbf{A}}(\mathbf{R}_j,\mathbf{R}_{j-1};\tau)=e^{-i(\mathbf{R}_j-\mathbf{R}_{j-1})\cdot\mathbf{A}((\mathbf{R}_j+\mathbf{R}_{j-1})/2)}, \tag{25}$$

$\mathbf{F}_Q=-\nabla_{\mathbf{R}}\ln\psi_G$ is the quantum force, and $\tilde{E}_L=\psi_G^{-1}(-\frac{1}{2}\nabla_{\mathbf{R}}^2+V+\boldsymbol{\sigma}\cdot\mathbf{B})\psi_G$ is the local energy of the guiding function *without* the contribution from the vector potential, which is taken into account by $G_{\mathbf{A}}$. One can verify that this G satisfies Eq. (21) for infinitesimal times τ by substituting it into the master equation Eq. (21) and performing a Taylor expansion for small $\mathbf{R}-\mathbf{R}'$, keeping only terms of linear order in τ. In this limit of short time steps the solution to Eq. (21) is equivalent to considering the local energy and quantum force as constant in the neighborhood of $\mathbf{R}$. The midpoint evaluation of the vector potential in $G_{\mathbf{A}}$ is necessary to obtain the correct form of the Schrödinger equation (a problem related to the Ito integral [18]).

B. Choice of the guiding function

Since the matrix elements depend upon the inverse of the guiding function ψ_G, it is essential, to avoid large statistical fluctuations, that our choice for ψ_G has no nodes that might be encountered by a random walk (or more correctly if the ratio Φ_i/ψ_G diverges at some value of $\mathbf{R}$, then it is possible that the variance will also diverge). This fact generally rules out simply assigning ψ_G to one of the basis states in the set $\{f_i\}$. We would like ψ_G to reflect the properties of the entire spectrum of ground and excited states in such a way that we can accurately calculate a number of states together. As shown in CB the minimization of the mean squared variance $\mathcal{V}(t)=\sum_{i=1}^{m}\nu_i(t)$ with respect to ψ_G, at small imaginary times, results in an expression for the optimal guiding function under certain assumptions. On the other hand, it was found useful in our released-node calculations of atoms to add a term to the guiding function proportional to the full electron density [19]. We have thus chosen to use the following form for the guiding function:

$$\psi_G(\mathbf{R})=C_\psi\left[c_0\prod_i\rho(\mathbf{r}_i)+\sum_{i=1}^{m}c_i|f_i(\mathbf{R})|^2\right]^{1/2}, \tag{26}$$

where $\rho=\sum_{k=1}^{N}|\psi_k|^2$ is the single state electron density derived from a Slater determinantal many-body wave function (ψ_k are the single particle orbitals coming from a mean-field calculation, for example, from HF). The coefficient C_ψ is added to make the normalization of ψ_G explicit. Note that if all of the states have a common node, then so will the guiding function. Adding this first term avoids this complication.

This form for ψ_G has a parameter governing the amount of overlap with any given state. We have also implemented a variational method for choosing the coefficients $\{c_i\}$ such that the sum of the variances of the individual states is minimized (this method is also used for generating the set of initial configurations distributed according to ψ_G^2). For the application considered below, however, the variances of the highest excitations dominate, so it is often possible (and faster) to tune the parameters $\{c_i\}$ by hand. In fact we do not believe that the above form is optimal, but it does appear satisfactory. If one chooses $c_0=0$ then there are unacceptable large fluctuations, particularly at stronger magnetic fields, due to the possibility of Φ_i/ψ_G becoming divergent.

C. Evaluation of expectation values

The computation of matrix elements other than the energy was not considered in CB; however, they are easy to obtain. Define the projected, orthogonalized basis functions as

$$\Phi_i(\mathbf{R},t)=\sum_{j=1}^{m} d_{ij}(t)\tilde{f}_j(\mathbf{R},t). \tag{27}$$

The projected basis functions converge exponentially fast to the exact functions

$$\lim_{t\to\infty}\Phi_i(\mathbf{R},t)=\Phi_i^{ex}. \tag{28}$$

To illustrate the general approach, consider the matrix element of a local scalar observable $\hat{O}(\mathbf{R})$ between two exact states Φ_α and Φ_β. The expectation value of such an operator which does not, in general, commute with the Hamiltonian can be computed as the large time limit of

$$\langle\alpha|\hat{O}|\beta\rangle=\int d\mathbf{R}\Phi_\alpha^*(\mathbf{R},t)\hat{O}(\mathbf{R})\Phi_\beta(\mathbf{R},t) \tag{29}$$

$$=\sum_{i,j=1}^{m} d_{\alpha i}^* d_{\beta j}\mathbf{O}_{ij}(t), \tag{30}$$

where writing in coordinate space we get

$$\mathbf{O}_{ij}(t)=\int d\mathbf{R}d\mathbf{R}'d\mathbf{R}''F_i^*(\mathbf{R})G(\mathbf{R},\mathbf{R}';t/2)\hat{O}(\mathbf{R}') \times G(\mathbf{R}',\mathbf{R}'';t/2)F_j(\mathbf{R}'')\psi_G^2(\mathbf{R}''). \tag{31}$$

This matrix is estimated using the same trajectory,

$$\mathbf{o}_{ij}(l\tau)=\frac{1}{p-l}\sum_{n=1}^{p-l} W_{n,n+l}F_i^*(\mathbf{R}_n)O(\mathbf{R}_{n+l/2})F_j(\mathbf{R}_{n+l}). \tag{32}$$

Hence the scalar is evaluated midway between the two end points. For convenience one takes l to be an even integer.

D. Summary of the numerical algorithm

To summarize the CF algorithm: (i) The basis states (typically from some other method such as a Hartree-Fock) and a set of desired projection times $\{l\tau\}$ are chosen. A set of initial configurations $\{\mathbf{R}_0\}$ is generated, distributed according to ψ_G^2.

(ii) A single configuration from the set $\{\mathbf{R}_0\}$ is evolved over a very large number (p) of time steps. At each time step the new configuration is chosen according to G_d (as in Ref. [1]). Instead of branching (as in diffusion Monte Carlo), we compute weights and evaluate correlation functions between the basis states. At each point along the walk, the quantities F_i, E_i, E_L, and W are stored into the past in a circular buffer whose length is determined by the longest desired projection time. The estimators **h** and **s** are updated according to Eqs. (14) and (15). At the end of the random walk, the matrix equation,

$$\mathbf{hd}_i=\lambda_i\mathbf{sd}_i \tag{33}$$

is solved for each projection time.

(iii) We repeat the preceding step for as many configurations N_T as desired. One can vectorize or parallelize to improve performance, by simultaneously evolving N_T walks in parallel, thereby obtaining completely independent estimations of the matrices **H** and **S** and independent estimates of the eigenvalues.

From the independent estimates of the eigenvalues one determines the variance and the bias in the eigenvalue. The bias arises because the eigenvalues are nonlinear functions of the quantities averaged. We have used the simplest form for the bias estimate [4],

$$b_i=\left(\sum_{\alpha=1}^{N_T}\lambda_i^\alpha/N_T-\Lambda_i\right)\Big/(N_T-1), \tag{34}$$

where Λ_i is determined from the averaged matrices, summed over the total number of trajectories N_T, each having eigenvalues given by $\{\lambda_i^\alpha\}$.

The variance grows exponentially with imaginary time as we shall explore further in Sec. III. Note that the points along each trajectory will be distributed according to $\mathcal{P}$, necessitating a careful choice of the guiding function ψ_G. An inappropriate guiding function will have little overlap with the desired states or could have a highly fluctuating weight factor.

III. APPLICATION TO ISOLATED HE ATOMS IN A MAGNETIC FIELD

The Hamiltonian in atomic units for an atom in a constant magnetic field of strength B is given by

$$\hat{H}=\sum_{i=1}^{N}\left[-\frac{\nabla_i^2}{2}-\frac{Z}{r_i}+\frac{\beta^2}{2}(x_i^2+y_i^2)\right]+\beta(\hat{L}_z+2\hat{S}_z) + \sum_{1\le i<j\le N}\frac{1}{r_{ij}}, \tag{35}$$

where $\hat{L}_z=\Sigma_{i=1}^N\hat{\ell}_{iz}$ and $\hat{S}_z=\Sigma_{i=1}^N\hat{s}_{iz}$ are the z component of the total angular momentum and spin of the system, respectively, and lengths are in units of the Bohr radius a_0. The magnetic field is parametrized by $\beta_Z=ea_0^2B/2\hbar cZ^2=B/B_0Z^2=\beta/Z^2$, where $B_0=4.7\times10^9$ G, and Z is the charge of the nucleus. We will focus on the ''strong'' field

regime, $10^{-2} \leqslant \beta_Z \leqslant 1$, where Coulomb and Lorentz forces are of equal importance, precisely the region of interest for astrophysical applications. We have chosen the magnetic field to be parallel to the z axis, and the symmetric gauge, which has vector potential $\mathbf{A}=B(-y,x,0)/2$. Later we will consider the implications of choosing another gauge.

In the absence of external fields, the eigenvalues of $\hat{L}^2$, $\hat{L}_z$, $\hat{S}^2$, $\hat{S}_z$, and parity, $\hat{\Pi}$, are good quantum numbers. When the magnetic field is turned on, the rotational invariance is broken and the only conserved quantum numbers are the eigenvalues of $\hat{L}_z$, $\hat{S}^2$, $\hat{S}_z$, and $\hat{\Pi}$ (alternatively, we will use the z parity $\hat{\pi}_z$). We will include the zero field designation of ground and excited states along with the strictly correct quantum numbers (L_z,π_z,S_z) to allow for an easier comparison with the more familiar zero field situation. For simplicity we only report calculations here for the quantum numbers $S=1$, $S_z=-1$, and $L_z=-1,0$ [11].

A. The basis states

When choosing basis states it behooves us to pick functions that most closely approximate the exact eigenstates. We have chosen to use wave functions arising from our recent Hartree-Fock (HF) calculations [12], multiplied by a standard [1] two-body Jastrow factor. They are the most accurate calculations, to date, of the ground and excited state spectrum of helium in strong fields. Since the HF wave functions are expansions in a basis set of Slater type orbitals, however, they suffer from inaccuracies due to finite basis set size. This finite basis size effect restricts the number of excitations of a given symmetry (about three) for which we can obtain good error bars ($\lesssim 10^{-3}$ hartree), and also limits the maximum field strength that we can study ($\beta_Z \sim 1$). Notice, however, that a different basis set $\{f_i\}$ could be chosen for $\beta_Z \gg 1$ using the adiabatic approximation. These limitations do not preclude an exact solution when RP is used, they only affect statistical fluctuations.

As mentioned above we have used the guiding function of Eq. (26). In general, c_0 is increased as the magnetic field strength is increased, due to the fact that the points at which the individual basis states vanish grow more confined. This behavior can be seen in Fig. 1, which shows the HF electron density for the first three states of symmetry $(L_z,\pi_z,S_z)=(0,+,-1)$ at both zero field (top) and $\beta_Z=0.1$ (bottom). Note that the strong field confines the electrons nearer to the nucleus, hence c_0 must often be increased to prevent numerical instabilities caused by common nodes among the basis states $\{f_i\}$. For the other coefficients, c_i $(i>0)$, one typically chooses ascending values (for example, $c_1=0.1$, $c_2=0.5$, $c_3=1.0$) such that the random walk also explores the region more distant from the nucleus. This choice helps sample more efficiently the more highly excited states, and avoids getting stuck in pockets of phase space.

B. Results for neutral He

As a test of our RP method we evaluated excited state energies for He at zero magnetic field strength. Comparison with extensive variational calculations of the nonrelativistic helium atom, which are essentially ''exact'' and with the experimental values gave complete agreement, showing the

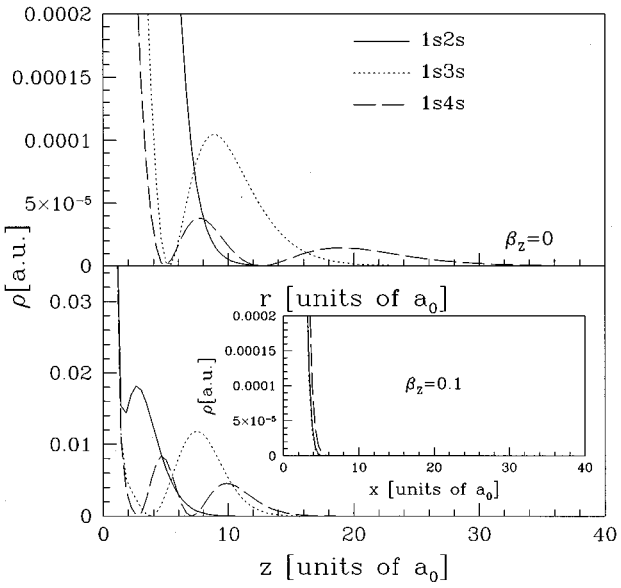

FIG. 1. The HF electron density (in atomic units) in the longitudinal (z) and transverse (x) directions for the first three excited states of neutral helium that are spherically symmetric at zero field (top plot). The bottom plot shows the resulting anisotropy in the electron density when a field of $\beta_Z=0.1$ is applied.

systematic errors to be smaller than our statistical errors. Relativistic and finite nuclear mass effects are also very small. We also tested that our RP procedure recovered the HF results at zero projection time, and that the results were

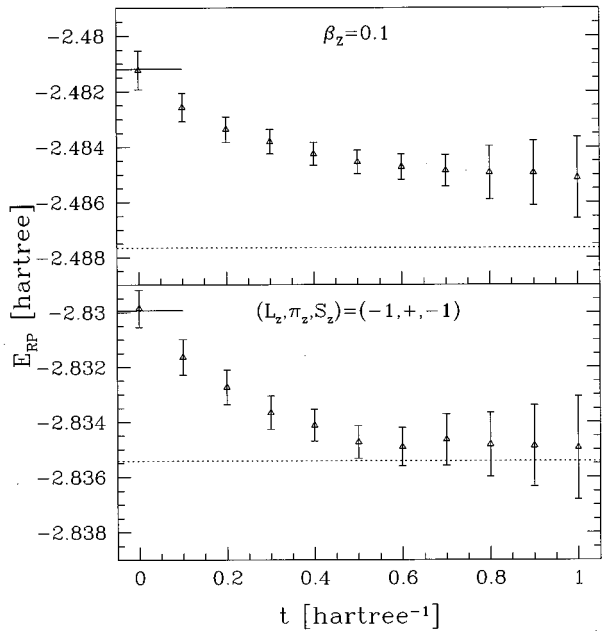

FIG. 2. A typical RP calculation for the helium atom ($1s2p_{-1}$ state) at $\beta_Z=0.1$, showing the convergence of the first two excited states in imaginary time. The dotted line indicates the fixed-phase results for that state. The FP value is in close agreement for the ground state, but is too low for the second state due to overlap with the lower state. This illustrates the nonvariational character of FP when applied to excitations. The short line segment at $t=0$ is the HF energy value.

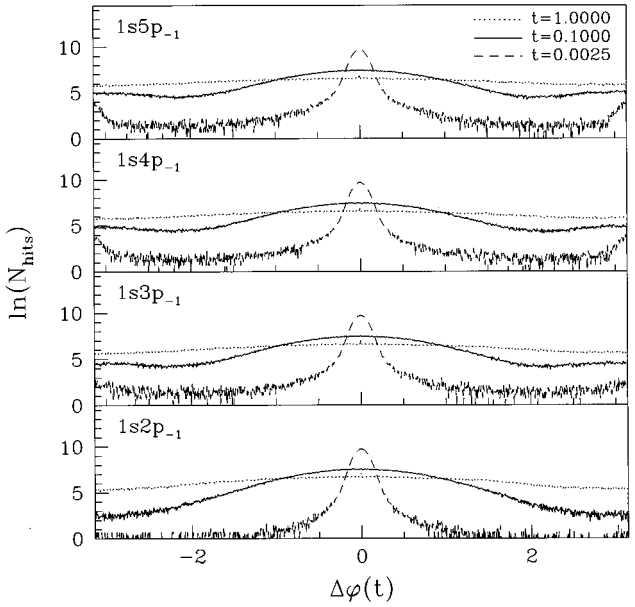

FIG. 3. The probability distribution $\Delta\varphi$ at three increasing values of imaginary time $t=0.0025$, 0.1, 1.0 for several excited states over the course of the random walk in a typical RP calculation, as defined in Eq. (36). N_{hits} is the number of points along the path taking on a particular value of $\Delta\varphi$. Note that broadening of the distribution occurs more rapidly for the higher excited states (top).

independent of time step. Further tests were performed on the excited state spectrum of neutral hydrogen atoms in strong fields. Using fairly crude approximations for the excited states we were able to recover the known energies of the low-lying excitations [10].

Turning now to strong magnetic fields, Fig. 2 shows the convergence of the first two excited states of the helium

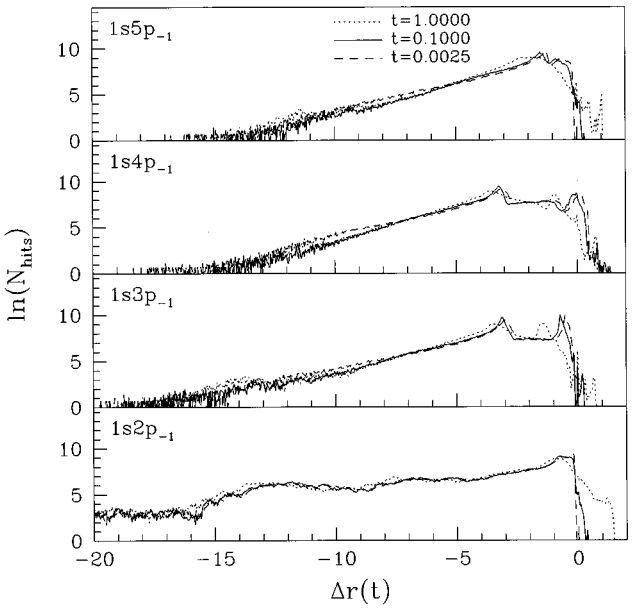

FIG. 4. The probability distribution Δr at three increasing values of imaginary time $t=0.0025$, 0.1, 1.0 for several excited states over the course of the random walk in a typical RP calculation, as defined in Eq. (36). Note that Δr shows little dependence on the imaginary time.

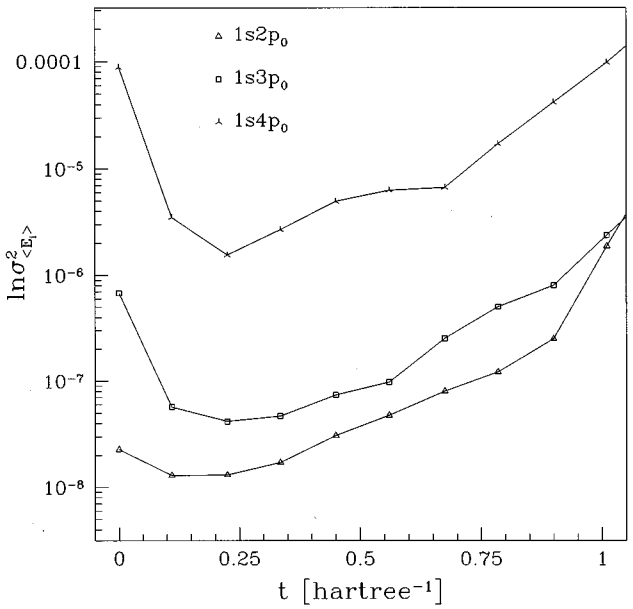

FIG. 5. The increasing variance as a function of projection time and excitation energy for the first three excitations of $(L_z,\pi_z,S_z)=(0,+,-1)$ symmetry in helium at $\beta_Z=0.3$. Zero field quantum numbers are given in the key at the top of the plot. Note that the variance of the energy, $\sigma^2_{\langle E_i\rangle}$, grows with projection time and excitation energy. The initial decrease in the variance is due to the improvement of the wave function at short imaginary times. The lines are provided only as a guide to the eye.

atom at $\beta_Z=0.1$ of the $(L_z=-1,\ \pi_z=+,\ S_z=-1)$ symmetry. In this example 50 independent trajectories each with a total time of 1.5 (atomic units) ($N_T=50$, $p=600\,000$, $\tau=0.0025$) were used. At zero time the energy is the variational energy, in this case the self-consistent-field HF energy of the first two basis states. As we progress in imaginary time the energy drops and the variance grows. The energy

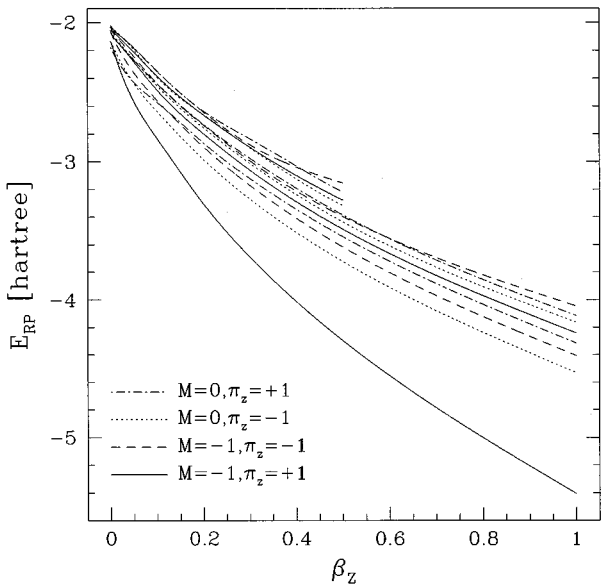

FIG. 6. The neutral helium energy spectrum using RP. The lines are spline fits to our data, included in Table I. Three states were evaluated for each of the four symmetries shown.

clearly converges before the variance gets too large.

The reason why the variance grows is shown in Fig. 3, which plots the change in the phase $\Delta\varphi$, of the first three excited states of symmetry $(L_z,\pi_z,S_z)=(-1,+,-1)$ at $\beta_Z=0.1$ for a sampling of elapsed times. Define the change in magnitude and phase for a particular state as

$$\Delta r + i\Delta\varphi_j(m\tau) = \ln[F_j^*(\mathbf{R}_n)W_{n,n+m}F_j(\mathbf{R}_{n+m})]. \quad (36)$$

Figure 3 shows a histogram of this phase change determined over the course of the random walk. Note the spreading of the phase with increasing imaginary time (the zero time value is simply a spike at zero). For this particular calculation, the longest time at which data could be meaningfully gathered was approximately $t=m\tau\simeq 1.0$. A similar plot for the magnitude (shown in Fig. 4) Δr, does not show the same behavior at increasing times, or with increasing excitation energy. This general result illustrates the fact that the dominant contribution to the increasing variance comes from the change in the phase. Figure 5 shows the typical behavior of the variance at long times for several excited states. Note that, as expected, the variance is much larger for the more highly excited states.

Figure 6 shows the energy spectrum for neutral helium, including the first three excited states of each symmetry having $L_z=0$ and $L_z=-1$. Note that the separation between states of the same symmetry grows larger as the field increases, and there are many level crossings as the field grows larger. At a zero applied field, our calculated energies reproduce the results of extensive variational calculations [20]. The data for the energies shown in Fig. 6 is included in Table I.

C. Accuracy of the HF and FP approximations

Using converged energies we are now able to determine the accuracy of the HF and fixed-phase approximations for atoms in strong magnetic fields. With increasing magnetic field strength, the errors in the HF energies grow due to the combination of basis set truncation error [12] and increasing electron correlation. Figure 7 shows the difference between the RP and HF results for the first three excitations of all four symmetries considered thus far. The truncation errors in the HF results make it difficult to isolate trends in the RP-HF differences. Since we therefore do not get the true HF energy, we can not accurately determine the correlation energy. The basis set errors are also the dominant contribution to the MC variances. Improved basis sets would lead to smaller error bars for our RP energies.

Figure 8 shows a comparison between the FP and RP energies for the two lowest states of all four symmetries considered thus far. We note that, within error bars, the FP and RP results are equal for the lowest symmetry state (lower plot) except for $\beta_Z=1$, implying that the fixed-phase ap-

TABLE I. RP energies, E_{RP}, for He in the $L_z=0, 1$, $S_z=-1$ states in hartree. Numbers in parentheses are the uncertainties for each energy. Quantum numbers (L_z,π_z,S_z) are at the top.

		$(0,+,-1)$				$(-1,+,-1)$	
	$1s2s$	$1s3s$	$1s4s$		$1s2p_{-1}$	$1s3p_{-1}$	$1s4p_{-1}$
β_Z	$-E_{\mathrm{RP}}$	$-E_{\mathrm{RP}}$	$-E_{\mathrm{RP}}$	β_Z	$-E_{\mathrm{RP}}$	$-E_{\mathrm{RP}}$	$-E_{\mathrm{RP}}$
0.0000	2.1751(6)	2.0687(2)	2.0365(1)	0.0000	2.1339(8)	2.0581(3)	2.0323(2)
0.0010	2.1830(5)	2.0760(1)	2.0413(4)	0.0010	2.1437(7)	2.0689(4)	2.0407(3)
0.0100	2.2438(3)	2.1209(1)	2.0687(9)	0.0100	2.2380(9)	2.1219(5)	2.0809(9)
0.1000	2.5737(3)	2.4395(9)	2.3497(21)	0.1000	2.8354(5)	2.4856(5)	2.3852(17)
0.2000	2.8669(5)	2.7330(8)	2.6665(26)	0.2000	3.3079(7)	2.8015(5)	2.6950(12)
0.3000	3.1225(5)	2.9751(11)	2.8357(29)	0.3000	3.6912(4)	3.0616(7)	2.8961(7)
0.4000	3.3460(3)	3.1912(13)	3.0400(26)	0.4000	4.0179(8)	3.2905(9)	3.1425(36)
0.5000	3.5429(8)	3.3855(11)	3.2197(10)	0.5000	4.3043(5)	3.4886(5)	3.2782(13)
0.7000	3.8902(5)	3.7069(31)		0.7000	4.7985(3)	3.8291(8)	
1.0000	4.3204(5)	4.1169(19)		1.0000	5.4072(13)	4.2436(32)	
		$(0,-,-1)$				$(-1,-,-1)$	
	$1s2p_0$	$1s3p_0$	$1s4p_0$		$1s3d_{-1}$	$1s4d_{-1}$	$1s5d_{-1}$
β_Z	$-E_{\mathrm{RP}}$	$-E_{\mathrm{RP}}$	$-E_{\mathrm{RP}}$	β_Z	$-E_{\mathrm{RP}}$	$-E_{\mathrm{RP}}$	$-E_{\mathrm{RP}}$
0.0000	2.1339(8)	2.0581(2)	2.0323(2)	0.0000	2.0557(8)	2.0315(9)	2.0198(9)
0.0010	2.1408(8)	2.0655(5)	2.0350(10)	0.0010	2.0672(9)	2.0413(9)	2.0266(7)
0.0100	2.2050(6)	2.1100(3)	2.0578(14)	0.0100	2.1410(1)	2.0912(2)	2.0624(9)
0.1000	2.6397(9)	2.4545(6)	2.3925(7)	0.1000	2.5590(27)	2.4369(12)	2.3504(14)
0.2000	2.9873(8)	2.7596(8)	2.6749(6)	0.2000	2.8964(7)	2.7394(8)	2.6436(17)
0.3000	3.2710(8)	3.0128(8)	2.9021(20)	0.3000	3.1714(5)	2.9946(11)	2.8785(16)
0.4000	3.5134(7)	3.2365(13)	3.1177(17)	0.4000	3.4075(9)	3.2092(13)	3.0307(30)
0.5000	3.7231(9)	3.4356(6)	3.3173(32)	0.5000	3.6188(20)	3.39670(21)	3.1640(31)
0.7000	4.0870(2)	3.7550(12)		0.7000	3.9756(8)	3.7203(20)	
1.0000	4.5314(4)	4.1651(8)		1.0000	4.4214(19)	4.1074(9)	

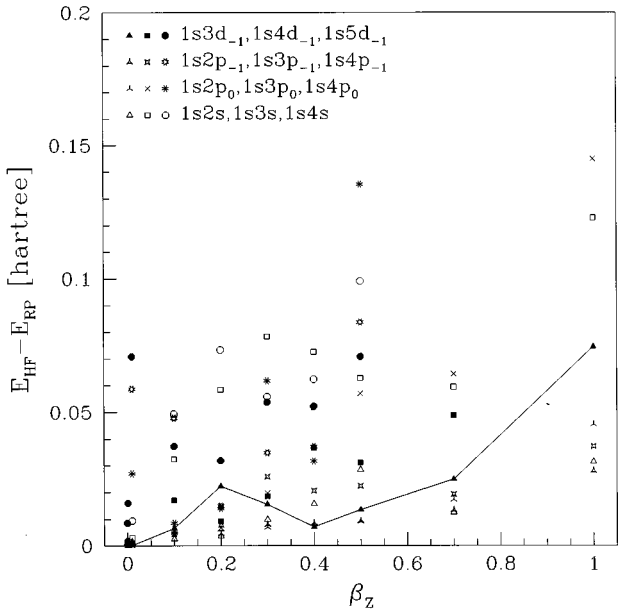

FIG. 7. Energy differences between the RP and HF results, for the first three excitations of all four symmetries $L_z=0,-1$, $S_z=-1$, $\pi_z=\pm$. Zero field quantum numbers are included in the key in the upper part of the plot. Error bars are approximately the same size (or smaller) than the symbols. The line connects the $1s3d_{-1}$ data (▲), and is provided only as a guide to the eye. The spread in the data points is due to the incomplete convergence of the HF calculations.

proximation is a good one for the lowest-lying excitations of the helium atom, at least over most of the range of magnetic field strengths studied thus far. The difference at larger values of β_Z can be attributed to the fact that the HF phase function is inadequate. We also note that the FP results for

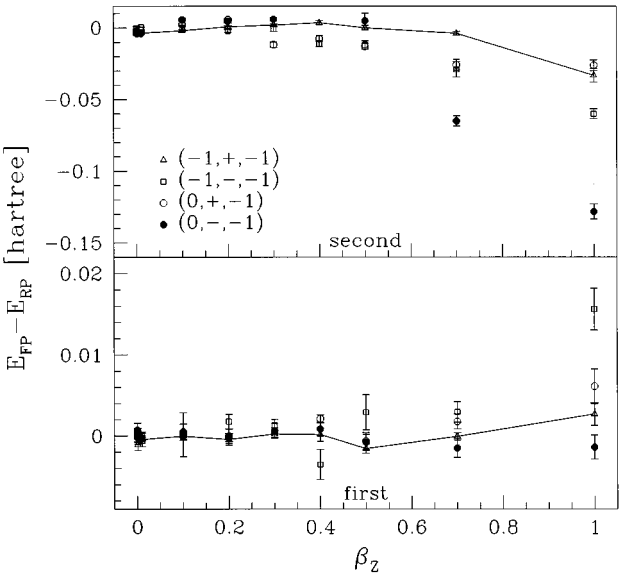

FIG. 8. A comparison between the FP and the RP results for the first two excited states of $(L_z,\pi_z,S_z)=(-1,\pm,-1)$ and $(0,\pm,-1)$ symmetry as a function of magnetic field strength. The line connects the points of $(-1,+,-1)$ symmetry, and is provided only as a guide to the eye.

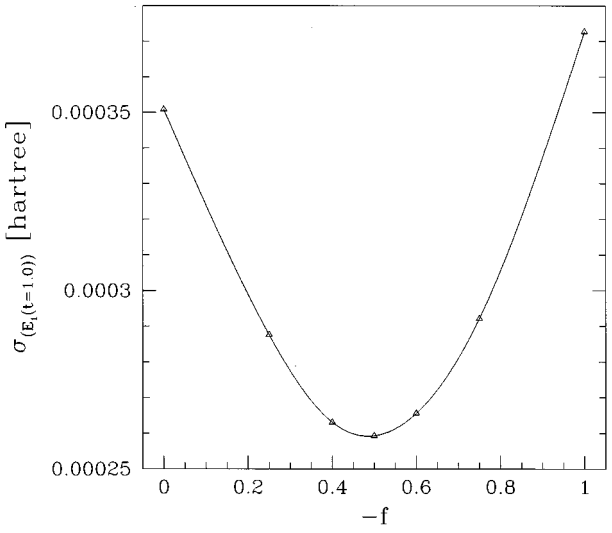

FIG. 9. Dependence of the variance on the gauge in a typical RP calculation. The vector potential is given by $\mathbf{A}=B(fy,(1+f)x,0)$. Shown is the variance of the energy of the first $(L_z,\pi_z,S_z)=(0,+,-1)$ state at $\beta_z=0.1$. The line is a spline fit to the data points (△).

the higher excited state (upper plot) are generally lower (but not uniformly lower) than the exact energies. Since FP is no longer variational for the more highly excited states of a particular symmetry, and the error is not very predictable, the RP method is necessary (and crucial) for an accurate determination of the excited state energies.

D. Gauge dependence

Thus far we have neglected the role of gauge freedom, and simply chosen to use the symmetric gauge $[\mathbf{A}=B(-y,x,0)/2]$ throughout. Certainly any physical observable must be independent of the choice of gauge, but it was suggested by Zhang, Canright, and Barnes [16] that the gauge could be used to lower the variance of the energy. The results of Zhang, Canright, and Barnes were based on lattice MC calculations for a tight binding model, for which they tested two choices of gauge, one of which varied considerably more than the other for a typical MC move. They found that the gauge which varied the least on average during the random walk (the gauge more evenly distributed over space) had MC averages with much smaller error bars.

It is clear, however, that the statistical variance is gauge invariant in the following sense. If we consider adding a many-body gauge and simultaneously change the phase of the basis set,

$$\mathbf{A}\rightarrow\mathbf{A}+\nabla\Lambda_{\mathbf{A}}, \tag{37}$$

$$f_i\rightarrow e^{-i\Lambda_{\mathbf{A}}}f_i, \tag{38}$$

the total contribution to the matrix elements will be invariant and, hence, the eigenvalues and variances will be unaffected. Hence, if the basis set is optimized (say within HF) for a given gauge, shifting the gauge will change nothing. If the basis set is nonoptimized or optimized for a different gauge, then a gauge transformation could have an effect.

There is another way the gauge could affect the efficiency. The accuracy of the short-time Green's functions [Eq. (22)] could depend on the gauge. We neglect commutators between the vector potential and the kinetic energy in making the Trotter breakup. Gauges with smooth values of **A** will have smaller time step errors.

We have tested the effect of the gauge for the helium atom by generalizing to an ''elliptic'' gauge (but still satisfying $\nabla \cdot \mathbf{A} = 0$),

$$\mathbf{A} = B(fy, (1+f)x, 0), \tag{39}$$

where $f = -1/2$ corresponds to the symmetric gauge. Figure 9 shows a series of RP calculations with various values for f for the $(L_z, \pi_z, S_z) = (0, +, -1)$ symmetry at $\beta_Z = 0.1$ and projection time $t = 1.0$. We see that the variance is minimized for $f \approx -1/2$, the symmetric gauge, with the largest variance at the extremes $f = 0$ and $f = -1$. This result is a demonstration that the symmetric gauge minimizes the variance when using our form for the short-time Green's function [Eq. (22)] and HF basis states.

IV. CONCLUSIONS

We have introduced the correlation function method to complex-valued wave functions. This released-phase method has a wide range of potential physical applications, of which we have selected magnetized atoms as an important example. We have thus been able to determine the ground and excited state spectrum of neutral helium in fields up to 10^{10} G with an unprecedented level of accuracy, a necessity for matching astrophysical observations of spectra from compact stellar remnants. The RP technique, however, is limited in its scope of application to small systems with relatively small excitation energies. By generating more accurate basis sets and guiding functions we hope to be able to apply this method to larger atoms such as carbon, for which accurate spectral calculations in strong magnetic fields do not yet exist. We will present more extensive improved RP calculations for neutral helium elsewhere [21], and discuss the relevance to the observed spectra [9]. Bayesian methods can also be used to aid in the extrapolation to large projection times [22]. Although we have implemented the RP method for particles in the continuum, the approach can easily be extended to fermions on a lattice.

ACKNOWLEDGMENTS

This work was supported by NSF Grant No. DMR-91-17822 and ONR Grant No. N00014-93-1029. Calculations were performed at the National Center for Supercomputing Applications (NCSA) and the Cornell Theory Center (CTC).

[1] P. J. Reynolds, D. M. Ceperley, B. J. Alder, and W. A. Lester, Jr., J. Chem. Phys. **77**, 5593 (1982).
[2] G. Ortiz, D. M. Ceperley, and R. M. Martin, Phys. Rev. Lett. **71**, 2778 (1993).
[3] F. Bolton, Phys. Rev. B **54**, 4780 (1996).
[4] D. M. Ceperley and B. Bernu, J. Chem. Phys. **89**, 6316 (1988).
[5] B. Bernu, D. M. Ceperley, and W. A. Lester, Jr., J. Chem. Phys. **93**, 552 (1990).
[6] Y. Kwon, D. M. Ceperley, and R. M. Martin, Phys. Rev. B **53**, 7376 (1996).
[7] M. P. Nightingale and H. W. J. Blöte, Phys. Rev. B **54**, 1001 (1996).
[8] J. D. Landstreet, in *Cosmical Magnetism*, edited by D. Lynden-Bell (Kluwer Academic, New York, 1994).
[9] G. D. Schmidt, W. B. Latter, and C. B. Foltz, Astrophys. J. **350**, 758 (1990); G. D. Schmidt, R. G. Allen, P. S. Smith, and J. Liebert, *ibid.* **463**, 320 (1996).
[10] G. Thurner, H. Korbel, M. Braun, H. Herold, H. Ruder, and G. Wunner, J. Phys. B **26**, 4719 (1993).
[11] It should be noted that, when using basis functions that are eigenfunctions of $\hat{L}_z$, the Hamiltonian [Eq. (35)] for a given sector of $\hat{L}_z$, the Green's function [Eq. (7)], and the resulting matrices [Eqs. (5) and (6)] can all be made real.
[12] M. D. Jones, G. Ortiz, and D. M. Ceperley, Phys. Rev. A **54**, 219 (1996).
[13] R. J. Elliott and R. Louden, J. Phys. Chem. Solids **15**, 196 (1960).
[14] Y. Wan, G. Ortiz, and P. Phillips, Phys. Rev. Lett. **75**, 2879 (1995).
[15] *Fractional Statistics and Anyon Superconductivity*, edited by F. Wilczek (World Scientific, Singapore, 1990); G. S. Canright, Int. J. Mod. Phys. B **5**, 2791 (1991).
[16] L. Zhang, G. Canright, and T. Barnes, Phys. Rev. B **49**, 12 355 (1994).
[17] J. K. L. MacDonald, Phys. Rev. **43**, 830 (1933).
[18] L. S. Schulman, *Techniques and Applications of Path Integration* (Wiley, New York, 1981), Chaps. 4 and 5.
[19] D. M. Ceperley and B. J. Alder, J. Chem. Phys. **81**, 5833 (1984).
[20] G. W. F. Drake, in *Long-Range Casimir Forces*, edited by F. S. Levin and D. A. Micha (Plenum, New York, 1993).
[21] M. D. Jones, G. Ortiz, and D. M. Ceperley (unpublished).
[22] M. Caffarel and D. Ceperley, J. Chem. Phys. **97**, 8415 (1992).